Chemical Engineering Science 65 (2010) 4931–4942

Contents lists available at ScienceDirect

Chemical Engineering Science

journal homepage: www.elsevier.com/locate/ces

Mass transfer limitations in slurry photocatalytic reactors: Experimental validation

María de los Milagros Ballari *, Orlando M. Alfano, Alberto E. Cassano

INTEC (Universidad Nacional del Litoral and CONICET), Colectora de la Ruta Nacional, No. 168, Km 472.5, Edificio INTEC I, 3000 Santa Fe, Argentina

ARTICLE INFO

Article history:
Received 8 October 2009
Received in revised form
29 March 2010
Accepted 16 April 2010
Available online 22 April 2010

Keywords:
Photochemistry
Chemical reactors
Slurries
Titanium dioxide
Mass transfer
Diffusive limitations

ABSTRACT

In the present work the existence of mass transfer limitations in slurry, photocatalytic reactors is studied. Experimental validation is made in a flat plate reactor that is part of a recycling system. The reactor is described with a mathematical model previously developed [Ballari et al., 2008a. Chemical Engineering Journal 136, 50], considering a transient, two-dimensional mass balance (TDM). The complete reactor model was developed to show the existence of these effects, which result from the occurrence of concentration gradients in reaction space. They develop when these reactors are operated under some operating conditions whose effects should be always analyzed before assuming the validity of existence of perfect mixing in reaction space. Dichloroacetic acid (DCA) was the adopted model compound. To solve TDM, a kinetic expression for DCA acid was determined before under well mixed conditions [Ballari et al., 2009. Industrial and Engineering Chemistry Research 48(4), 1847]. The studied variables are flow rate, catalyst loading, and irradiation rates. The experimental data agree quite well when they are interpreted in terms of the two-dimensional model (TDM) regardless of the operating mode. The perfect mixing model (PMM), normally employed to describe this and other types of slurry photoreactors, does not have the same level of universal application; i.e. it is restricted to perfect mixing, but in many cases far simpler to use. However, it can be concluded that when the photocatalytic reaction is not fast, employing catalyst loadings below 1 g L^{-1}, irradiation rates at the reactor wall below 1×10^{-6} Einstein cm^{-2} s^{-1} and good mixing operation ($Re>1700$) it will be always safe to assume that mass transport limitations in the bulk of the fluid are nonexistent. In a typical batch reactor the above flow conditions are equivalent to very intense mixing. If the catalyst concentration is increased, the mixing conditions should be improved in the same proportion. Within limits, higher solid loadings can be compensated with lower irradiation rates [Ballari et al., 2008a. Chemical Engineering Journal 136, 50]. In addition, with the validated model, additional simulations are shown, operating the reactor under different virtual reactor thicknesses to widen amplitude of the reached conclusions. These findings will be useful in kinetic studies to prevent incursion in certain ranges of experimental conditions that could lead to erroneous interpretation of the obtained kinetic data.

1. Introduction

Increasing concern with environmental deterioration has been an important incentive to promote research in new methods to degrade undesired pollutants in both air and water. Some of them are known as Advanced Oxidation Technologies (AOTs) and, among them, there is an important working line that uses UV radiation. These technologies, most of them still in the process of development, have some important advantages that, without exhausting the list, can be listed as follows: (1) they are destructive, rendering almost always innocuous end products; i.e. they do not translate the pollution from one phase to another as is the case of activated carbon adsorption or air stripping and (2) they are mostly non-selective; thus, they can be used for a wide range of undesirable compounds (Bahnemann,1999; Chen et al., 1999; Choi et al., 2007; De Lasa et al., 2005; Malato et al., 2003; Matthews, 1986, 1991; Ollis and Pellizzetti, 1991).

Heterogeneous photocatalysis employing UV radiation, oxygen (or air), and a solid semiconductor catalyst such as titanium dioxide is one of the most intensively studied processes (Hoffmann et al., 1995). Radiation of the required wavelength (below 390 nm for typical titania) can activate the catalyst, generating separation of charge carriers that are able to produce reductive and oxidative pathways by themselves or giving rise to highly reactive radicals such as $HO^{\cdot}$ that proceed with the mineralization reaction.

Mass transfer limitations have been extensively analyzed in several forms of immobilized TiO_2, either external to solid surfaces (typically, the boundary layer of catalytic films) or in its internal structure (Camera-Roda and Santarelli, 2007;

* Corresponding author. Tel.: +54 342 4511546; fax: +54 342 4511087.
E-mail address: ballari@santafe-conicet.gov.ar (M.d. Ballari).

0009-2509/$ - see front matter © 2010 Elsevier Ltd. All rights reserved.
doi:10.1016/j.ces.2010.04.021

Chen et al., 2000, 2001; Dijkstra et al., 1999, 2001a, 2001b, 2002, 2003; Dionysiou et al., 2002; Edwards et al., 1996; Goetz et al., 2009; Ray and Beenackers, 1997; Sclafani et al., 1993; Subramanian et al., 2003; Turchi and Ollis, 1988; Zhou and Ray, 2003). Conversely, the case of slurry reactors has been much less examined and only a few contributions can be quoted. Employing a simplified reaction and radiation model, Bideau et al. (1994) published a rather limited work, whose conclusions are of restricted validity. Some time later, Chen and Ray (1999), working with suspended solid reactors, reported that they did not find diffusive limitations either intra- or extra particle. With a simple kinetics, performing research in an annular reactor, and employing a rigorous theoretical approach, Martin et al. (1999) found these effects after changing optical thickness of reaction space, which resulted in changes in global photonic absorption rate and in reactor conversion. They reported a loss in reactor efficiency when the optical thickness of the suspension exceeded an optimum calculated value. Mehrotra et al. (2003) found experimentally that for large catalyst loadings there are both mass and radiation transport restrictions inside the catalytic particle, providing some qualitative explanation for their results. More recently, Peralta Muniz Moreira et al. (2005), adopting a pseudo-first order kinetic law, used the classical Weiz and Prater criterion to determine the rate controlling step of the reaction with the result that no diffusion limitations for the reaction existed.

At the same time, there are many contributions related to experimental observations that found different catalyst concentration limits beyond which reaction rate reaches a plateau or decreases appreciably. In fact, there is no agreement concerning the optimum value to be employed in photocatalytic reactions carried out in diverse configurations of slurry reactors, even if using the same semiconductor brand and the same model compound (Ahmed and Ollis, 1984; Bangun and Adesina, 1998; Fabiyi and Skelton, 1999; Gonçalves et al., 1999; Ilisz et al., 1999; Li Puma and Yue, 1999; Salinaro and Serpone, 1999; Serpone, 1997; Stafford et al., 1997; Turchi and Ollis, 1989; Wei and Wan, 1991). Moreover, when the liquid substrate competes for radiation absorption, concentrations of Degussa P 25 in the order of $15\times10^{-3}\,\mathrm{g\,cm^{-3}}$ have been found to be necessary to reach reasonable values of mineralization (Sagawe et al., in press).

The problem of mass transport phenomena influencing the rate is important, both for laboratory studies in order to obtain intrinsic reaction kinetic parameters as well as for photoreactor design to improve operation efficiency. Also, this issue is important in those cases in which a laboratory reactor of noticeable size is agitated with conventional magnetic stirring and the experimental results are analyzed in terms of a perfectly mixed reactor.

In this work we will attempt to make an experimental validation of a mathematical model described in Ballari et al. (2008a), which predicts the presence of these limitations when some of the operating conditions favor the existence of concentration gradients in the reaction space. With this objective, different experiments were made in a photoreactor operating in a recycle and the following were analyzed: (1) employing intermediate to low recirculation flow rates that might render mixing conditions deficient, (2) changing catalyst loading, (3) varying irradiation rates, and finally (4) performing additional runs to eliminate the disguising potential of results due to damping or mitigation effects produced by the large liquid volume in the tank, employing a reduced quantity of suspension in the reservoir. In the experiments indicated in (1) and (2), a high degree of irradiation was applied in order to enhance reaction rates and induce the presence of mass transfer constraints. However, a few runs were made at low irradiation rates but using high catalyst loadings and at low flow rates, in order to also study the effect of these variables on possible mass transport limitations.

Taking into account the operating conditions in the laboratory work, the transient, two-dimensional mass balance (the TDM model) developed by Ballari et al. (2008a) was used. In this conservation equation, the degradation kinetics of DCA previously studied was incorporated (Ballari et al., 2009). In the latter, experiments were made under controlled, perfect mixing conditions. In the present work, for comparison purposes, results obtained with the perfect mixing model (PMM) also will be always reported in order to observe under which conditions this assumption loses its validity. These results will also be very useful to ensure that all the results published by Ballari et al. (2009), even under extreme operating conditions, were obtained under circumstances where a perfect mixing state prevailed.

Finally, employing the validated kinetics and reactor model, simulations were made with the TDM model for other different hypothetical reactors where some of their characteristics were modified; for example, employing the same area of radiation entrance, changing reactor thickness, and observing results in the predicted DCA conversion. In a forthcoming work, internal particle limitations, either in mass transport or in radiation penetration will be experimentally studied to complete validation of the published theoretical models in Ballari et al. (2008b).

2. Experimental reactor

2.1. Reacting system

The experiments were carried out in a specially designed and built photoreactor, which is part of a batch recirculation system. As shown in Fig. 1 (with all details in Table 1) the device consisted of the following parts. (1) The reactor. It was a prism having rectangular ends and rectangular sides made of stainless steel. The large height of the parallelepiped permitted ensuring of a fully developed flow profile when the reactor was operated in the laminar flow regime. The actual photoreactor was at the top, where two small rectangular windows made of borosilicate glass were allocated on each side. The transmission characteristics of this glass in the useful wavelength range of interest have been measured and reported in Fig. 2(a). (2) The irradiating system. It was made of several components. (i) Two high power UV lamps located at each side of the reactor; the wavelength relative distribution of the output power of each lamp was precisely known and is also reported for the employed useful wavelength range of this work in Fig. 2(a). It must be noted that only a fraction of its output power was useful for the employed catalyst and hence in the figure $\Sigma_\lambda f_\lambda \neq 1$. (ii) Two custom made cylindrical reflectors of parabolic cross section, made of aluminum mirrors. Each lamp was located horizontally at the focal axis of each reflector. (iii) Between each lamp–reflector system and the reactor window, a fixed plate made of borosilicate ground glass was located in order to produce diffuse irradiation. (iv) A sliding shutter was placed between the flat plates and the reactor windows in order to decide on the exact moment to commence the reaction after reaching steady state in all parts of the apparatus. (v) The possibility of interposing, right after the shutter, neutral density filters of different transmission characteristics to vary the irradiation rates arriving at the windows of radiation entrance. (vi) Operating temperatures of the lamps and the reflectors were adjusted and controlled with variable flow rate air currents produced by powerful blowers. (3) A stainless steel recirculating centrifugal pump with an incorporated electronic flow rate control. (4) A calibrated rotameter. (5) A perfectly stirred tank, made of glass. The tank was fully isolated from the laboratory lights and had provisions for: (i) temperature control; (ii) sampling, and (iii) an additional circuit in order to improve mixing. (6) A long, all glass, heat exchanger for temperature control connected to a thermostatic bath was operated. (7) An oxygen saturation system with a glass

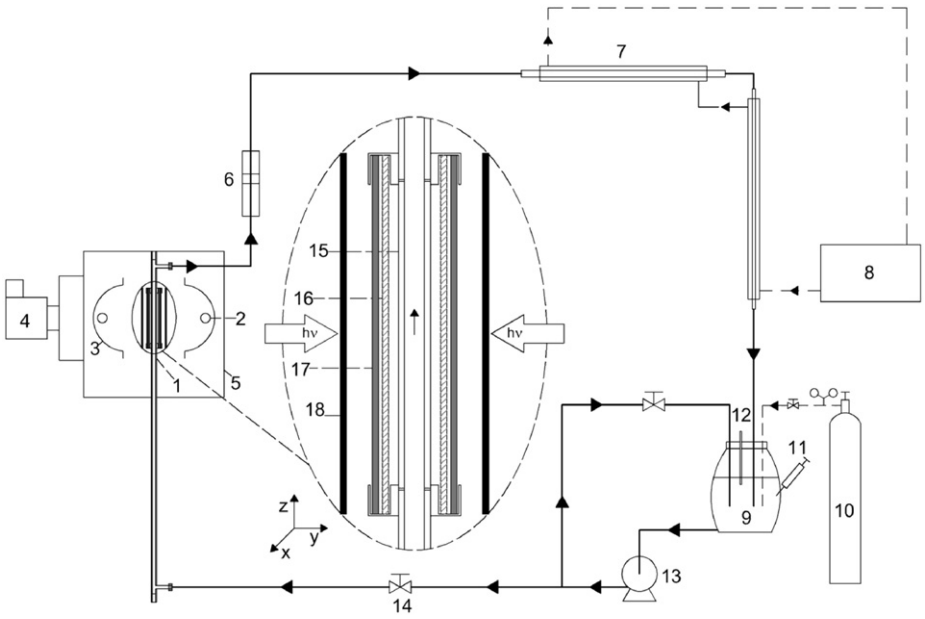

Fig. 1. Reactor description. Keys: 1, reactor; 2, UV lamp; 3, parabolic reflector; 4, fan; 5, box; 6, flowmeter; 7, heat exchanger; 8, thermostatic bath; 9, tank; 10, oxygen supply; 11, sampling; 12, thermometer; 13, pump; 14, valve; 15, borosilicate glass window; 16, borosilicate ground glass; 17, neutral filter; 18, shutter.

Table 1
Detailed characteristics of the experimental set-up.

Reactor	Length	100 cm
Made of stainless steel	Entrance length	75 cm
	Width	8 cm
	Thickness	1 cm
	Total volume	800 cm^3
Photoreactor windows	Length	15 cm
Made of borosilicate glass	Width	8 cm
Photoreactor volume		120 cm^3
Total suspension volume		4000 cm^3
Tank	Maximum volume	5000 cm^3
Made of glass		
Lamps: one on each side	Input power	1000 W
Philips HPA 1000	Emission wavelength	260–580 nm
	Length	8.5 cm
Parabolic reflectors	Focal distance	2.78 cm
Made of aluminum specularly	Aperture	20 cm
Finished mirrors with Alzac® treatment	Length	14 cm
Filters	Transmittance	20%
Made of stainless steel mesh		
Recirculating pump	Total maximum flow rate	182 $cm^3 s^{-1}$
Made of stainless steel		
	Reactor operation maximum flow rate	76 $cm^3 s^{-1}$
Tubing	Diameter	0.95 cm
Made of stainless steel		

disperser acting inside the tank to maintain a constant concentration of dissolved gas in the reacting suspension. (8) A large box enclosing the entire reacting system to protect the operator. All connections in the circuit were made with stainless steel tubing.

3. Reactants, analytical procedures, and operating conditions

3.1. Reactants

The employed reactants during the photocatalytic experiments were DCA Merck (purity $>98\%$) and oxygen (industrial quality purity $>99.5\%$).

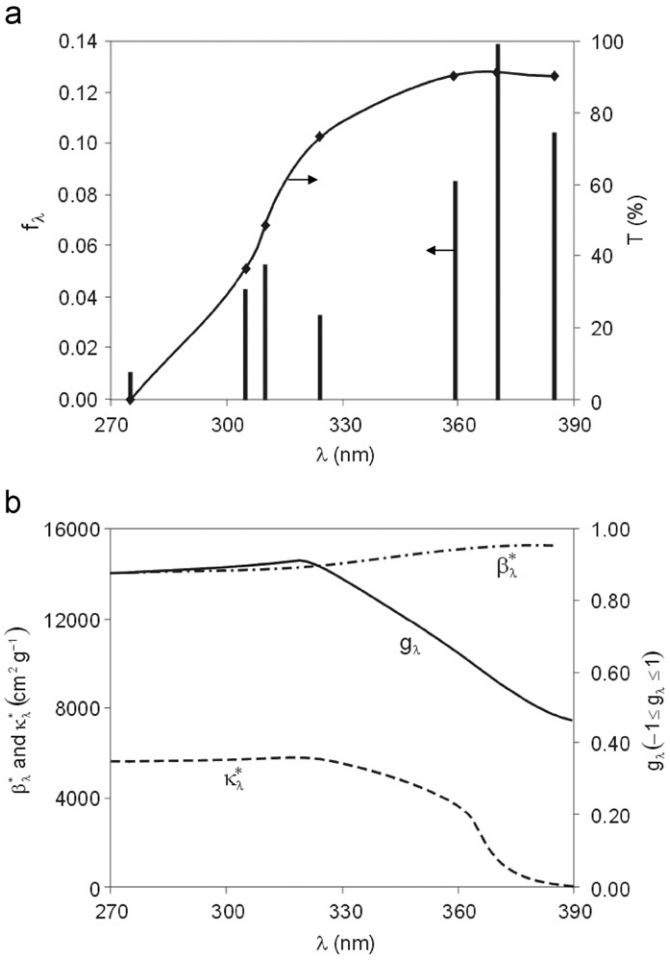

Fig. 2. (a) Left: spectral distribution of UV lamp emission lines. Right: percent transmission of borosilicate glass windows. (b) Left: specific extinction and absorption coefficients. Right: asymmetry factor of the HG phase function for scattering.

3.2. Catalyst

Considering the objectives of this work, it was decided to employ Aldrich titanium dioxide (99% Anatase) having a nominal elementary particle size of 200 nm and a specific surface area of $S_g = 9.6\,m^2\,g^{-1}$. It is clear that its catalyst efficiency is lower than that of the more widely used Degussa P 25. Had we decided to employ this variety of titania, the eventual existence of mass transfer limitations would have been more notorious. However, these results would have been obtained at the price of a much more significant uncertainty in the quality of the data, because titanium deposition at the reactor windows is much more severe with this catalyst and it is impossible to avoid. It is worth mentioning that employing TiO_2 Degussa P25 would increase even more the chance of mass transfer limitation since it presents higher photocatalytic activity (Preis et al., 1997), higher specific surface area (Cabrera et al., 1996), and larger radiation absorption characteristics (Satuf et al., 2005).

In order to correctly characterize the radiation field and solve the Radiative Transfer Equation (RTE), optical properties of the catalyst must be known. For the operating conditions employed in this work, and the useful emission lines of the used lamp, they can be extracted for the data published by Satuf et al. (2007) and are summarized in Fig. 2(b). The value of g corresponds to the asymmetry factor of the adopted model for scattering known as the Henyey and Greenstein (HG) phase function model (Siegel and Howell, 2002; Van de Hulst, 1980):

$$p_{HG,\lambda}(\mu_0) = \frac{(1-g_\lambda^2)}{(1+g_\lambda^2-2g_\lambda\mu_0)^{3/2}} \quad (1)$$

In Eq. (1) μ_0 is the cosine of the angle between the directions of propagation of the ray resulting from scattering and that for which the RTE is written.

3.3. Analysis

In every sample, dichloroacetic and chloride ion concentrations were analyzed in triplicate employing ion exchange chromatography (using $1.7\times10^{-6}\,mol\,cm^{-3}$ $NaHCO_3$ and $1.8\times10^{-6}\,mol\,cm^{-3}$ Na_2CO_3 as eluents, an IonPack AG4A-SC column, a Waters 432 conductivity detector, and an Alltech DS-Plus suppressor column). These results were always compared with total organic carbon content, employing a TOC-5000A Shimadzu equipment, in order to achieve two different purposes: (1) to measure the degree of mineralization and (2) to verify the closure of mass balance and the absence of stable, reaction intermediates, transforming the DCA disappearance data to equivalent information corresponding to TOC concentration as well as comparing these results with the equivalent chloride ion concentration appearance. Spectrophotometric measurements for the potassium ferrioxalate actinometry were made by employing an UV–visible Cary 100 Bio apparatus.

3.4. Operation

After cleaning the experimental device, the titanium dioxide suspension and the DCA solution were loaded; the oxygen feed, the system flow rate, and temperature were stabilized, keeping the latter at 20 °C. For each run, the desired flow rate was adjusted by employing the calibrated rotameter. This operation took between 30 and 50 min. Then, the lamps were turned on and stabilized for 20 min (while the shutters on the reactor windows were on; i.e. no radiation was entering into the reactor). Then, the sample at $t=0$ min was taken at the same time that the lamp shutters were taken off. Afterwards, samples were taken every 30 min for the above mentioned analytical measurements. The total reaction time was 3 h for all experiments. Every time an operating condition was changed, reproducibility of the results was verified. In this study pH of the suspension containing DCA was equal to 3. When low flow rates were employed, the combination of both factors induced agglomeration of the catalytic particles. In these cases, during the system operation accumulation of titanium dioxide was observed in some regions of the experimental set-up, reducing the actual catalyst load in the reaction zone. Therefore, in every run, a gravimetric determination of titanium dioxide content in a sample taken from the recirculating suspension was performed, in order to determine the exact catalytic concentration that was operating inside the photoreactor. Table 2 describes the operating conditions for every performed experiment and results of catalyst loading at the reactor exit given by the gravimetric determination.

4. Theoretical models

Details of the theoretical model have been described in a previous contribution (Ballari et al., 2008a, 2008b, 2009). In this section, only the final results will be presented.

4.1. Momentum balance

From momentum balance, under laminar regime and a well developed velocity profile:

$$v_{z,S}(y) = v_{max}\left[1-\left(\frac{2y}{H_R}-1\right)^2\right] \quad (2)$$

Table 2
Typical experimental data.

Experiment	$C_{mc,0}\times10^3\,g\,cm^{-3}$ [a]	$C_{mc}\times10^3\,g\,cm^{-3}$ [b]	$Q\,(cm^3\,s^{-1})$	$C_A^0\times10^6\,mol\,cm^{-3}$	Irradiation level %
1	1.00	1.00	76	1	100
2	2.00	2.00	76	1	100
3	2.00	1.75	36	1	100
4	3.00	2.75	36	1	100
5	2.00	1.70	23	1	100
6	3.00	2.50	23	1	100
7	2.00	1.50	13	1	100
8	3.00	2.20	13	1	100
9	3.00	2.40	13	1	20
10[c]	3.00	2.50	13	1	100

[a] Initially fed to the experimental set-up.
[b] Measured at the photoreactor exit.
[c] Total volume of the system reduced to $V_T = 2500\,cm^3$.

where

$$v_{max} = \frac{3Q}{2H_R W_R} \tag{3}$$

4.2. Mass balance

4.2.1. Two-dimensional model (TDM)

Mass balance of component "A" (DCA) in a continuous, laminar flow regime, applying a transient two-dimensional model, considering constant temperature, density, viscosity, and diffusivity results in (Ballari et al., 2008a)

$$\frac{\partial C_{A,R}(y,z,t)}{\partial t} + v_{z,S}(y)\frac{\partial C_{A,R}(y,z,t)}{\partial z} - \mathcal{D}_{A,mix}\frac{\partial^2 C_{A,R}(y,z,t)}{\partial y^2} = a_V \eta_0 R_{het,A,R}(R_P,y,z,t) \tag{4}$$

To derive Eq. (4) initially, the heterogeneous reaction has been considered as a boundary condition. Afterwards, employing $a_V = S_g C_{mc}$, the solid–liquid interfacial area per unit reactor volume, the pseudo-homogeneous assumption has been applied to incorporate reaction rate into the differential equation. In the mass inventory, the pseudo-binary diffusivity ($\mathcal{D}_{A,mix}$) for very dilute concentrations of DCA in water was determined employing different predictive models (Reid et al., 1987). A value of $\mathcal{D}_{A,mix} = 8.7 \times 10^{-6}\ cm^2\ s^{-1}$ was adopted for all calculations. For the employed catalyst concentrations, solid hold-up can be safely neglected. The global effectiveness factor η_0 inside the titanium dioxide particles agglomerations is defined as (Ballari et al., 2008b)

$$\eta_0 = \frac{\langle R_{V_P,A}[C_A(r),\ e^a_S(r)]\rangle_{V_P}}{R_{V_P,A}[C^s_A(R_P),\ e^a_S(R_P)]} = \underbrace{\frac{\langle R_{V_P,A}[C_A(r),\ e^a_S(r)]\rangle_{V_P}}{\langle R_{V_P,A}[C^s_A(R_P),\ e^a_S(r)]\rangle_{V_P}}}_{\eta_{diff}\left(\begin{smallmatrix}\text{diffusive mass transfer}\\ \text{effectiveness factor}\end{smallmatrix}\right)} \underbrace{\frac{\langle R_{V_P,A}[C^s_A(R_P),\ e^a_S(r)]\rangle_{V_P}}{R_{V_P,A}[C^s_A(R_P),\ e^a_S(R_P)]}}_{\eta_{att}\left(\begin{smallmatrix}\text{photon transport}\\ \text{effectivenes factor}\end{smallmatrix}\right)} \tag{5}$$

where $R_{V_P,A} = a_{V_P} R_{het,A}$ is the DCA reaction rate per unit volume of the agglomerate formed from the elemental particles and $a_{V_P} = S_g \rho_S (1-\varepsilon)$ the solid–liquid interfacial area per unit particle volume. The effectiveness factor can be calculated by solving mass balance inside the cluster and assuming spherical shape for the solid agglomerate (Ballari et al., 2008b). Additionally, the local superficial rate of photon absorption inside the porous agglomeration of elemental particles can be calculated, according to Ballari et al. (2008b), from

$$e^a_S(r) = \frac{e^a_\lambda[(y),\ C_{mc}]}{S_g C_{mc}} \frac{R_P}{r} \frac{\sinh(\gamma r)}{\sinh(\gamma R_P)} \frac{1}{\frac{3}{\gamma R_P}\left[\frac{1}{\tanh(\gamma R_P)} - \frac{1}{\gamma R_P}\right]} \tag{6}$$

where $\gamma^2 = 3(1-\omega_P)\beta^2_P$.

Making use of the effectiveness factor it is possible to work with properties of bulk of the suspension without consideration of internal structure of the solid accumulation. It is worth noting that Eq. (4) is valid for the case where no external mass transfer resistances are present. For typical catalyst particle agglomerations formed by titanium dioxide, Ballari et al. (2008b) have shown that they can be safely neglected.

From the results obtained by Ballari et al. (2009), effectiveness factor is not altered during the course of the reaction but it is very different from one due to the significant influence produced by photon transport limitations inside the cluster of elemental particles. The calculated value is $\eta_0 = 0.324 \pm 0.014$ valid for a wide range of operating conditions.

Mass balance in the tank for a heterogeneous system is

$$\frac{dC_{A,tk,ex}(t)}{dt} = \frac{Q}{V_{Tk}}[C_{A,tk,in}(t) - C_{A,tk,ex}(t)] \tag{7}$$

Initial and boundary conditions for the system are

$$C_{A,R}(y,z,t=0) = C^0_{A,R} \tag{8}$$

$$\frac{\partial C_{A,R}(y=0,\ z,\ t)}{\partial y} = 0 \tag{9}$$

$$\frac{\partial C_{A,R}(y=H_R,z,t)}{\partial y} = 0 \tag{10}$$

The coupling boundary conditions between the reactor and the tank are

$$C_{A,R,in}(y,z=0,t) = C_{A,tk,ex}(t) \tag{11}$$

$$C_{A,tk,in}(t) = \langle C_{A,R,ex}(y,\ z=L_R,\ t)\rangle_{A_R} = \frac{\int_{y=0}^{y=H_R} C_{A,R}(y,z=L_R,t)v_{z,S}(y)dy}{\int_{y=0}^{y=H_R} v_{z,S}(y)dy} \tag{12}$$

4.2.2. Perfectly mixed model (PMM)

Operation of the entire system can be analyzed employing a perfect mixing model (PMM) when the following conditions are satisfied: (1) differential conversion per pass, (2) very good mixing in the tank, and (3) the ratio $V_R/V_T \ll 1$. The last condition is in fact not necessary if the first is completely fulfilled. This model can be used to compare its predictions with the TDM model. The result is

$$\frac{dC_{A,tk}(t)}{dt} = \frac{V_R}{V_T} a_V \langle R_{het,A}(r,\ y,\ t)\rangle_{A_{S,R}} = \frac{V_R}{V_T} a_V \eta_0 \langle R_{het,A}(R_P,\ y,\ t)\rangle_{A_{S,R}} \tag{13}$$

where

$$C_{A,tk}(t=0) = C^0_A \tag{14}$$

The solution of parabolic differential equations [Eqs. (4) and (8)–(11)] for the reactor was numerically obtained using a Crank–Nicholson finite difference method. On the other hand, mass balance for the tank [Eqs. (7) and (12)] and the limiting case of the perfect mixed model [Eqs. (13) and (14)] were solved with a Runge–Kutta algorithm.

4.3. Kinetic expression

According to Ballari et al. (2009), where a photocatalytic kinetic study with a mechanistically based reaction model of DCA degradation was carried out, the following reaction kinetic model corresponding to DCA mineralization is employed:

$$a_v R_{het,A}(y,\ z,\ t) = C_{mc} S_g \alpha_1 C_A(y,\ z,\ t)\left\{1 - \sqrt{1 + \frac{2\alpha_2 \int_\lambda e^a_\lambda[(y),\ C_{mc}]d\lambda}{C_{mc} S_g C_A(y,\ z,\ t)}}\right\} \tag{15}$$

The following parameters were estimated by Ballari et al. (2009) from experimental data obtained under perfect mixing conditions:

$$\alpha_1 = (38.89 \pm 2.14) \times 10^{-7}\ cm\ s^{-1} \tag{16}$$

$$\alpha_2 = (1.64 \pm 0.35) \times 10^5\ mol\ s\ Einstein^{-1}\ cm^{-1} \tag{17}$$

4.4. Radiation balance

For any kinetically controlled photochemical reaction the LVRPA $[e^a_\lambda[(y),\ C_{mc}]]$ is the most critical parameter to calculate.

In this system the Radiative Transfer Equation (RTE) must take into account absorption as well as scattering. At the usual employed temperatures in photocatalytic systems, spontaneous or induced emission can be neglected. Then (Cassano et al., 1995; Özisik, 1973):

$$\frac{dI_{\lambda,\underline{\Omega}}(s,t)}{ds}+\underbrace{\kappa_\lambda(s,t)I_{\lambda,\underline{\Omega}}(s,t)}_{\text{absorption}}+\underbrace{\sigma_\lambda(s,t)I_{\lambda,\underline{\Omega}}(s,t)}_{\text{out-scattering}}$$
$$=\underbrace{\frac{\sigma_\lambda(s,t)}{4\pi}\int_{\Omega'=4\pi}p(\Omega'\to\Omega)I_{\lambda,\underline{\Omega}'}(s,t)d\Omega'}_{\text{in-scattering}} \quad (18)$$

For the case of slab geometry described in Fig. 3, considering the existence of azimuthal symmetry resulting from diffuse irradiation of the reactor windows, the RTE can be well approximated by the one-dimensional (y)–one-directional (θ) radiation model (the One-Dim–One-Dir model) originally proposed by Alfano et al. (1994):

$$\mu\frac{dI_\lambda(y,\mu)}{dy}+(\kappa_\lambda+\sigma_\lambda)I_\lambda(y,\mu)=\frac{\sigma_\lambda}{2}\int_{\mu'=-1}^{\mu'=1}I_\lambda(y,\mu')p(\mu,\mu')d\mu' \quad (19)$$

In Eq. (19) $\mu=\cos\theta$.

The diffuse and isotropic inlet boundary conditions are

$$I_\lambda(y=0,\mu)=I_\lambda^0 \quad \text{for } \mu>0 \quad (20)$$

$$I_\lambda(y=H_R,\mu)=I_\lambda^{H_R} \quad \text{for } \mu<0 \quad (21)$$

The boundary conditions at both windows can be obtained experimentally. For this purpose, values of total radiative flux $q_{W,T}$ on each side of the reactor windows, with and without filters, were measured with potassium ferrioxalate actinometry (Murov et al., 1993). The method was applied for the entire lamp emission wavelength range ($275\,\text{nm}\le\lambda\le580\,\text{nm}$), though only a fraction of it is useful for photocatalyst activation ($275\,\text{nm}\le\lambda\le390\,\text{nm}$). The exact amounts of radiation that can activate the catalyst were obtained from experimental measurements in the corresponding wavelength range according to the method described by Zalazar et al. (2005). They are shown in Table 3. From these values,

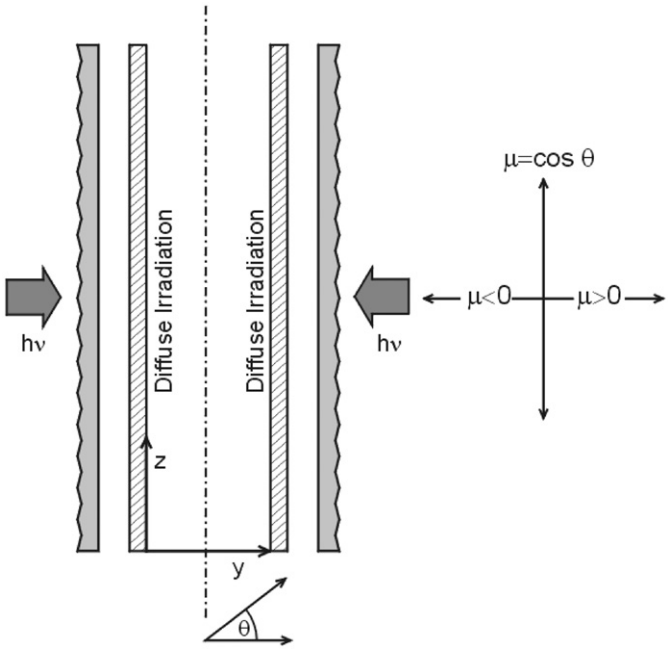

Fig. 3. Schematic representation of the One-Dim–One-Dir Model for radiation field inside the reactor.

Table 3
Boundary conditions for the RTE.

Reactor windows	Irradiation level (%)	$q_{w,T}\times10^6$ Einstein $cm^{-2}\,s^{-1}$
Right lamp	100	1.13
Left lamp	100	1.11
Right lamp with filter	19.16	0.22
Left lamp with filter	19.90	0.22

monochromatic boundary conditions are obtained according to Brandi et al. (2003) from

$$I_\lambda^0=\frac{(q_{W,T})_0\ f_\lambda\ T_\lambda}{\pi}\ \text{ and }\ I_\lambda^{H_R}=\frac{(q_{W,T})_{H_R}f_\lambda T_\lambda}{\pi} \quad (22)$$

The solution of Eqs. (19)–(21) was numerically obtained with the Discrete Ordinate Method (Duderstadt and Martin, 1979). From the values of specific intensities, for the One-Dim–One-Dir Model, the local volumetric rate of photon absorption (LVRPA) is simplified to

$$e_\lambda^a[(y),C_{mc}]=\kappa_\lambda\left\{2\pi\int_{\mu=-1}^{1}I_\lambda[(y,\mu),C_{mc}]d\mu\right\} \quad (23)$$

5. Results

5.1. Origin of the problem: experimental evidence

In photocatalytic reactions a special feature of photochemical reactions is very much enhanced. This is so due to the unavoidable non-uniformity of radiation field caused by photon absorption produced by titanium dioxide. This phenomenon occurs along trajectories of light beams, together with the inherent impossibility of achieving good mixing of highly reactive, short-lived, unstable reaction intermediates. This non-uniformity is distinctive of photoreactors and, as a consequence, of some of the existing concentration fields. With the exception of diffusion controlled overall rate processes, rate of photochemical reactions depends on the value of spectral rate of photon absorption per unit reaction volume, i.e. the local volumetric rate of photon absorption—$LVRPA=e_\lambda^a(\underline{x})$, indicating that it is a function of position x. Consequently, the unavoidable spatial non-uniformity of photon concentration and that of most of the short-lived reaction intermediates results in a non-uniform spatial distribution of reaction rates of stable species, even in well-mixed reactors from a strictly hydrodynamic point of view.

The conclusion is that even under conditions of good mixing all photochemical reaction rates are a function of position through their dependence on e_λ^a, due to radiation absorption by the dispersed catalysts present at every point in the reaction volume. This occurrence has a precise dependence on catalyst concentration and can be easily shown even in a reactor of very short optical thickness in the direction of characteristic length of radiation propagation, as in our reactor, where $H_R=1$ cm. Fig. 4 depicts the LVRPA profiles $[e_{\Sigma\lambda}^a(y)]$ inside the reactor as a function of reactor thickness (y) for several catalyst concentrations that were employed in different experiments and for a value corresponding to 100% of incident radiation. In the case of titanium dioxide, this effect is slightly attenuated at acidic conditions (caused by the employed reactant) according to the significant influence exercised by pH of the reacting medium (Satuf et al., 2005, 2007). As will be shown below, under some operating conditions, these non-uniformities are still maintained even for stable reaction species, giving rise to diffusive limitations.

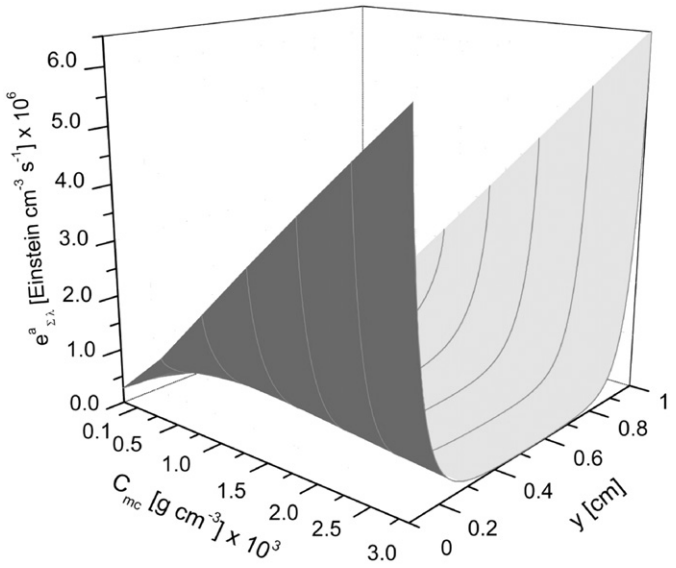

Fig. 4. Three-dimensional representation of the LVRPA as a function of main characteristic dimension for radiation propagation inside the reactor space and catalyst concentration.

5.2. Preliminary experiments

Prior to the specific photocatalytic experiments, DCA adsorption in the whole system was verified developing a dark run (UV lamps off) employing a concentration of $C_{mc}=1\times10^{-3}\,g\,cm^{-3}$. The DCA concentration remains invariant over time ($t=0$ min, $C_A=1.00\times10^{-6}\,mol\,cm^{-3}$; $t=60$ min, $C_A=1.02\times10^{-6}\,mol\,cm^{-3}$; $t=120$ min, $C_A=0.99\times10^{-6}\,mol\,cm^{-3}$), which permits neglect of DCA adsorption by different materials that form part of the experimental device.

In contrast with our previous work (Ballari et al., 2009), in this case, experimental runs were performed in the laboratory varying the main parameters that influence the photocatalytic reaction and can intensify mass and photon transfer limitations (Ballari et al., 2008a). Some typical runs are shown in Table 2. These parameters are high catalyst mass concentration, flow rates never reaching the turbulent flow regime, and rather high incident irradiation level. In all these experiments, the initial contaminant concentration was fixed at 1.0×10^{-6} mol cm^{-3}. In addition, to inspect the effect of low irradiation, the typical Run No. 9 was done with incident radiation of 20%. Finally, in order to exclude any sort of disguising results produced by the large tank volume, the effect was also analyzed with special experiments (typical Run No. 10) employing a total suspension volume smaller than the one used in the rest of the experiments (2500 cm^3).

In Table 4 some of these experimental results are shown in terms of DCA concentration measured by HPLC, the equivalent stoichiometrically produced chloride ion measured by ion chromatography expressed in terms of DCA concentration, and the equivalent TOC measurements also transformed in DCA concentrations; i.e. all of these determinations are expressed as DCA concentrations. Good agreement between the three concentrations can be observed. It can be seen that DCA degradation does not produce stable organic intermediates, because the DCA concentration chromatographically determined is almost equal to the DCA concentration in terms of equivalent TOC measurements. In addition, it can be concluded that the reaction stoichiometry was satisfied, because 1 mol of DCA generated 2 mol of chloride ion.

Table 4
Experimental results of DCA concentration evolution in the tank.

Time (min)	$C_{A,tk}\times10^6$		
	DCA concentration (mol cm^{-3})	Cl$^-$ DCA stoichioimetric equivalent (mol cm^{-3})	TOC DCA equivalent (mol cm^{-3})
0	0.975	0.975	1.065
30	0.676	0.714	0.718
60	0.442	0.466	0.463
90	0.287	0.276	0.261
120	0.153	0.160	0.142
150	0.087	0.080	0.077
180	0.047	0.048	0.048

$C_{mc}=2.20\times10^{-3}\,g\,cm^{-3}$; $Q=13\,cm^3\,s^{-1}$; $C_A^0=1\times10^{-6}\,mol\,cm^{-3}$; irradiation level: 100%.

5.3. Comparison of experimental results and models simulations

In what follows experimental values will be compared with results obtained by simulations employing the TDM and the PMM. All obtained experimental results shown here were made at the same initial concentration of DCA ($C_A^0=1\times10^{-6}\,gcm^{-3}$). Unless specifically pointed out, the first set of experiments were made with the same total reactor volume ($V_T=4000\,cm^3$) and the same irradiation intensity (100%). Changes were made only in flow rate and catalyst concentration. Fig. 5(a) and (b) shows two limiting conditions. In the first case (typical Run No. 1) the catalyst concentration is rather low ($1.0\times10^{-3}\,g\,cm^{-3}$) and the flow rate was the maximum tolerated by the experimental device without undesirable consequences to the photoreactor windows ($76\,cm^3\,s^{-1}$). In the second (typical Run No. 8) the catalyst concentration was higher, but not extremely high when compared to many usually employed loadings ($C_{mc}=2.2\times10^{-3}\,gcm^{-3}$) and low flow rate ($13\,cm^3\,s^{-1}$). In the first case it can be seen that the differences are minimal even though one could conclude that the TDM predicts results that are slightly closer to the data. In Ballari et al. (2008a) simulations have shown that in order to obtain a much better agreement it is necessary to raise flow rate to values at least twice higher than those employed here. Even more, in flow reactors where fully developed turbulent flow operation (Re=22,140) is achieved, these mass transfer limitations can be assumed completely negligible (Ballari et al., 2008a). In the second case deviations are significant and the PMM clearly separates from the experiments. In Fig. 5(a), the absence of differences between both models can be explained with the results of concentration profiles of DCA shown in Fig. 6(a) for typical Run No. 1. In this plot high flow rates and low catalyst loading can be observed and, consequently for considerable low conversions, the profile is almost flat. This occurs even under laminar flow conditions, excluding the regions very close to the wall, where the liquid velocity is zero. The opposite effect is even more significantly exhibited in Fig. 6(b) corresponding to typical Run No. 10 (see details in Table 2). Here, the operating conditions are very different and concentration gradients are very significant even for not too large conversions and the departure of the PMM from the experimental data is broader as will be displayed later. Notice that in this case $V_T=2500\,cm^3$. In the next paragraphs it will be seen that this reduction also influences the observed outcome.

The results shown here in Figs. 5(a) and 6(a) give more confidence to the intrinsic parameters of the kinetic model employed in this work. In fact, all experiments that took place to render the expression and data indicated in Eqs. (15)–(17), as

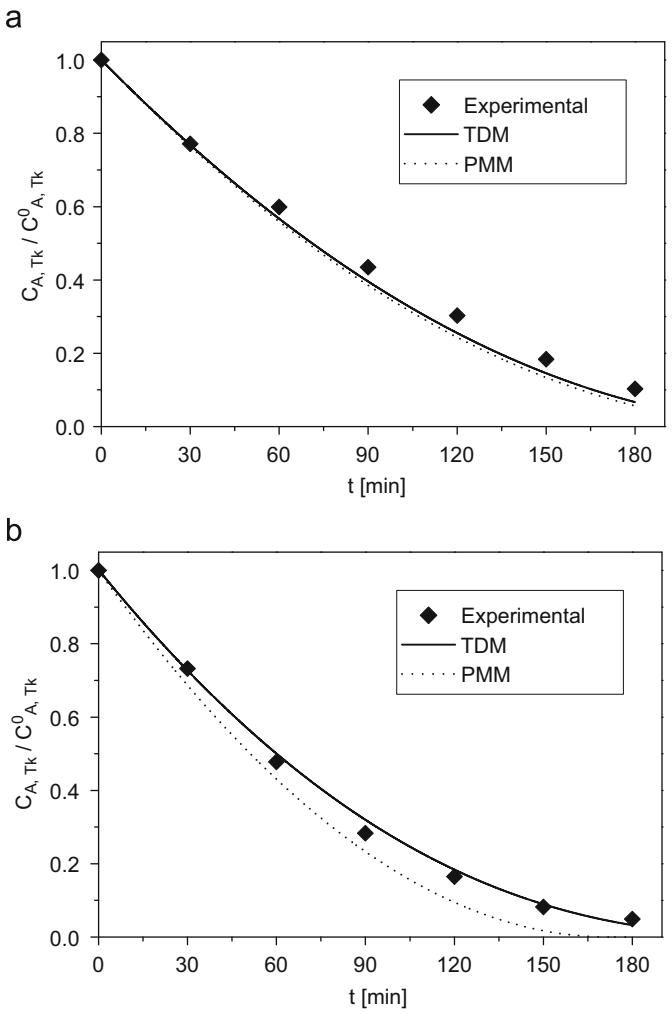

Fig. 5. Tank DCA concentration evolution. $C^0_A = 1 \times 10^{-6}$ mol cm^{-3}. Irradiation level: 100%. (a) $Q = 76$ cm^3 s^{-1}; $C_{mc} = 1.0 \times 10^{-3}$ g cm^{-3}. Run No. 1. (b) $Q = 13$ cm^3 s^{-1}; $C_{mc} = 2.20 \times 10^{-3}$ g cm^{-3}. Run No. 8.

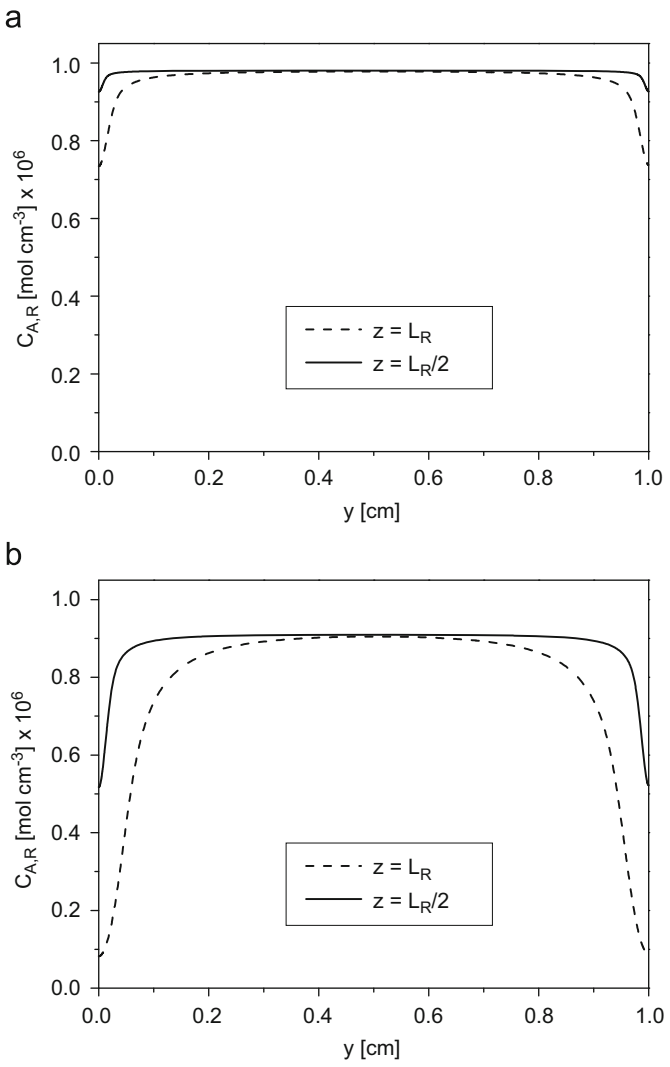

Fig. 6. Reactor concentration profiles of DCA as a function of reactor depth. $C^0_A = 1 \times 10^{-6}$ mol cm^{-3}; Irradiation level: 100%. (a) $V_T = 4000$ cm^3; $Q = 76$ cm^3 s^{-1}; $C_{mc} = 1.0 \times 10^{-3}$ g cm^{-3}; $t = 60$ s. Run No. 1. (b) $V_T = 2500$ cm^3; $Q = 13$ cm^3 s^{-1}; $C_{mc} = 2.5 \times 10^{-3}$ g cm^{-3}; $t = 60$ s. Run No. 10.

far as mixing conditions, catalyst concentrations, and irradiation rates are concerned, were obtained always under conditions even more favorable than those presented in typical Run No. 1 (Ballari et al., 2009).

Fig. 7(a) and (b) provides very useful information for designing laboratory reactors when the objective is to obtain meaningful kinetic data. The first one shows that even while working with low flow rates (13 cm^3 s^{-1}, Re = 288) and high catalyst concentrations (2.40×10^{-3} g cm^{-3}), it is only necessary to reduce significantly the irradiation rate (20% of the original irradiance rate) in order to almost approach the PMM operation and avoid significant mass transfer control (typical Run No. 9). According to the simulations reported in Ballari et al. (2008a), only a flow rate higher than 50 cm^3 s^{-1} (Re = 1100) is sufficient to reach the PMM behavior using 10% of the irradiation rate (1×10^{-7} Einstein cm^{-2} s^{-1}), employing catalyst loading up to 3 g L^{-1}. However, employing 100% of the irradiation rate (1×10^{-6} Einstein cm^{-2} s^{-1}), resorting only to Re numbers larger than 1700 ($Q = 76$ cm^3 s^{-1}), and catalyst loadings below 1 g L^{-1}, the mass transfer limitations can also be avoided. Conversely, Fig. 7(b) shows how a poor design of the experimental device (typical Run No. 10) makes mass transfer control even more distinguishable. In this case, it is evident that the conversion per pass in the photoreactor is not exceedingly small as desired and since V_T (2500 cm^3) is not appreciably large as compared with V_R as it was in previous experiments, the effect of this (relatively high) conversion per pass in the reactor is not attenuated by reduced tank volume. In addition, this performance departs even more from the behavior of the whole reactor system from the assumptions of the PMM.

This problem under consideration can be analyzed in terms of the value of the total percent root-mean-square error (RMS error) of all experimental data, for concentrations of DCA larger than 0.1 mM. It is defined as

$$\text{RMS error } [\%] = \sqrt{\frac{\sum_{i=1}^{N} \left(\frac{C^i_{A,\text{experimental}} - C^i_{A,\text{model}}}{C^i_{A,\text{experimental}}} \times 100 \right)^2}{N}} \tag{24}$$

Partial results for each typical run are shown in Table 5. It can be observed that for the TDM the values are almost constant for all experimental runs. Conversely, for the PMM when the operating conditions depart from those of a well mixed system and specially combined with high catalyst concentration and the maximum irradiation rate, error increases up to an intolerable magnitude. From these errors it is confirmed that for the maximum employed flow rate, errors are about the same with both models. If one takes

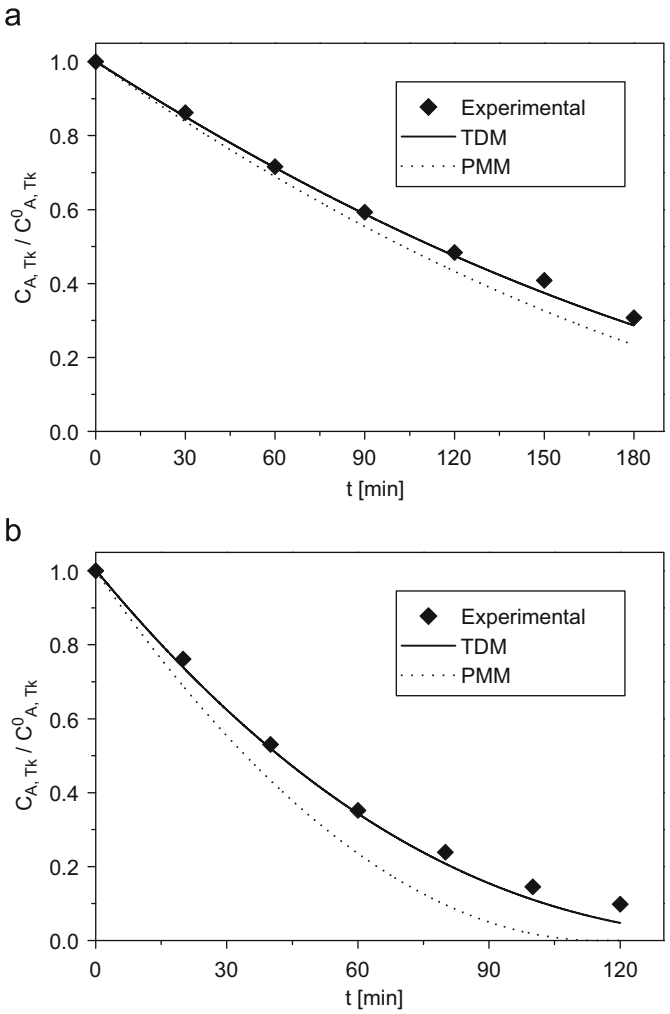

Fig. 7. Tank DCA concentration evolution. $C^0_A = 1 \times 10^{-6}$ mol cm^{-3}. (a) $V_T = 4000$ cm^3; Irradiation level: 20%; $Q = 13$ cm^3 s^{-1}; $C_{mc} = 2.40 \times 10^{-3}$ g cm^{-3}. Run No. 9. (b) $V_T = 2500$ cm^3; Irradiation level: 100%; $Q = 13$ cm^3 s^{-1}; $C_{mc} = 2.50 \times 10^{-3}$ g cm^{-3}. Run No. 10.

into account all experimental data the RMS error for the TDM is 8.62% whereas for the PMM the value is 21.89%.

A better way of showing the agreement between experimental data and results of the simulations with the TDM is to plot values of DCA concentrations in the tank predicted by the model simulations and the actual experimental data. The regressed straight line of these values should give a slope equal to one and the ordinate intercept should be equal to zero. Fig. 8 shows the results. In the case of the TDM this condition is well satisfied.

The relative difference between the TDM and PMM models is shown in Fig. 9. This three-dimensional plot indicates the relative errors between the models as a function of reaction time and recirculating flow rate for a catalyst concentration of 3×10^{-3} g cm^{-3}. They were calculated according to

$$\text{error}\,[\%] = \left| \frac{C_{A,TDM}(t) - C_{A,PMM}(t)}{C_{A,TDM}(t)} \right| \times 100 \qquad (25)$$

Notice that 3×10^{-3} g cm^{-3} is a concentration that is very often used in many kinetic studies in laboratory reactors. The condition mentioned before for absence of errors in the PMM pointing out specifically to the need for rather high flow rates, has its correlation in simple batch reactors that must be operated under very good mixing conditions, a requisite not always satisfied with mild magnetic stirring, particularly in rather large laboratory reactors.

Table 5
Errors resulting from the analysis of the results with both models.

Experiment	Error with TDM (%)	Error with PMM (%)
1	11.41	14.64
2	6.45	9.90
3	4.24	14.93
4	8.71	22.79
5	9.83	17.95
6	10.39	18.43
7	8.07	14.14
8	8.06	21.19
9	4.16	12.83
10	11.27	45.96

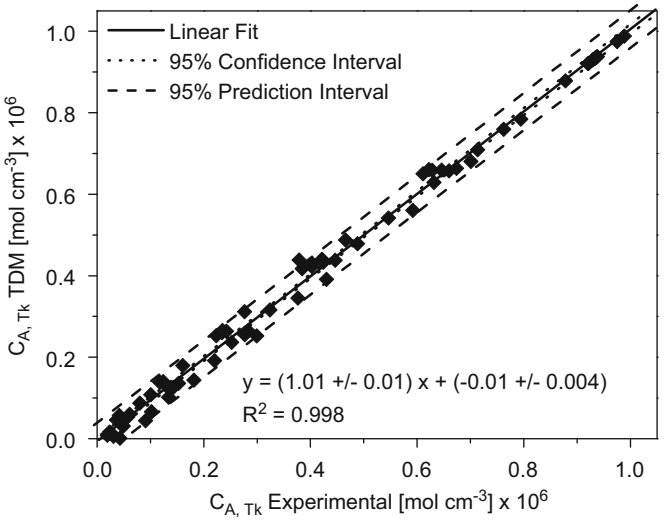

Fig. 8. DCA concentrations simulated by the TDM model versus experimental DCA concentrations. Linear regressions with the corresponding confidence intervals.

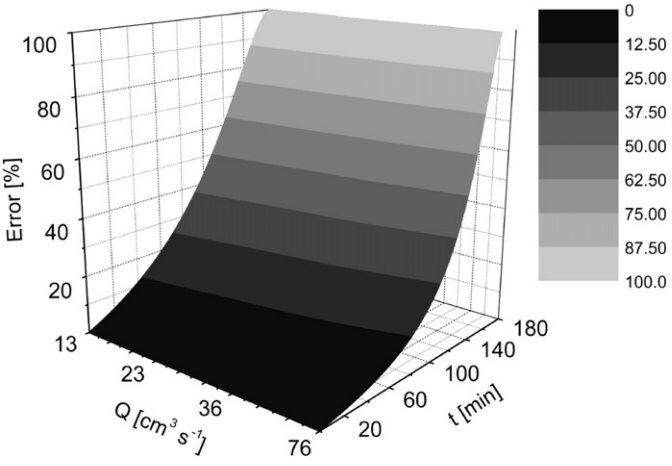

Fig. 9. Relative errors between the TDM and PMM models as a function of time and flow rate. $C^0_A = 1 \times 10^{-6}$ mol cm^{-3}; Irradiation level: 100%; $C_{mc} = 3.0 \times 10^{-3}$ g cm^{-3}.

One important message that can be deduced from these results is that for kinetic studies there are four factors that influence the application of the simple PMM. (1) Reaction rate for a given chemical system and a chosen catalyst is already fixed. Sometimes, some freedom can exist with the choice of the last. Let us consider the usual case where the rate is neither very fast nor very slow. Then, we are left with three variables. (2) Catalyst

concentration. (3) Irradiation rate. (4) Mixing conditions. The last should always be as intense as possible. Regarding catalyst loading and irradiation rate, the decision is the result of a trade-off analysis. For a maximum yield one should choose the largest tolerable values. However, considered separately, both maxima can lead to mass transport limitations. Then, either one of them or both will have to be reduced to the point where the problem is removed because both operate in the same direction. There is no unique numerical answer. In the case of this work, with catalyst concentration in the order of $1\times10^{-3}\,g\,cm^{-3}$ the maximum irradiation rate can be used. However, if the catalyst concentration is increased above this value, unless the flow rate is dramatically changed to very large Reynolds numbers, the irradiation rate must be reduced almost in the same proportion. Generally, this is an economical decision.

6. Simulations employing reactors of different thicknesses

Computer experiments will be made employing both models for the following operating conditions: $C_{mc}=3\times10^{-3}\,g\,cm^{-3}$, $Q=13\,cm^3\,s^{-1}$, and irradiation level equal to 100%. In these virtual experiments reactor thickness will be varied while maintaining the same reactor width and length. Fig. 10 shows results for three different cases. The larger the reactor thickness the broader the separation of one model from the other in predicting DCA conversion. In these simulations, two factors contribute to explain the differences: (1) on increasing reactor thickness the region that receives less radiation intensities is enlarged and concentration profiles in the "*y*" direction become more pronounced and (2) since reactor cross section is increased but reactor width is kept constant, fluid velocity becomes diminished in an equivalent proportion. Both effects contribute to reactor efficiency and to the fulfillment of good mixing conditions demanded by the PMM. In fact, this model predicts the same conversion for all thicknesses. Conversely, the TDM recognizes these changes and shows the expected differences.

7. Conclusions

In the present work, experimental validation of a transient two-dimensional reactor–reaction description (the TDM) is done. This model can predict the appearance of mass transfer limitations under certain operating conditions of a slurry photocatalytic reactor that affects degradation rate of the contaminant (DCA). These constraints affecting the kinetic control regime proceed from concentration gradients existing in the reaction space. However, they originate in the irreducible non-uniformities in the radiation field. Several experiments were carried out in the laboratory under different operating conditions that could lead to intensification of mass transfer limitations. With these experimental data and with a kinetic expression for the pollutant (DCA) determined under perfect mixing conditions, mass balance was coupled with a one-dimensional–one-directional radiation model to calculate photon absorption rate. This model can be used due to the incorporation in the experimental device of a ground glass plate that produces diffuse irradiation and hence renders azimuthal symmetry to the entering radiation. The reaction rate in this mass balance was affected by an effectiveness factor considering mass and photon transfer restrictions inside the particle agglomeration of titanium dioxide. This limitation is mainly due to radiation transfer constrains inside the usually formed agglomerates by titanium dioxide elemental particles. For the operating conditions in this study the effectiveness factor is low and remains nearly constant along the reaction. A very good correlation between experimental data and computer simulations with the theoretical TDM was obtained, with a total root mean square error equal to 8.62%. On the other hand, the extensively used perfect mixing model (PMM) presents a total root mean square error equal to 21.89% under operating conditions that were chosen on purpose, to favor the appearance of contaminant concentration gradients in the reactor. These conditions can be summarized as follows: (1) high catalyst loading (sometimes

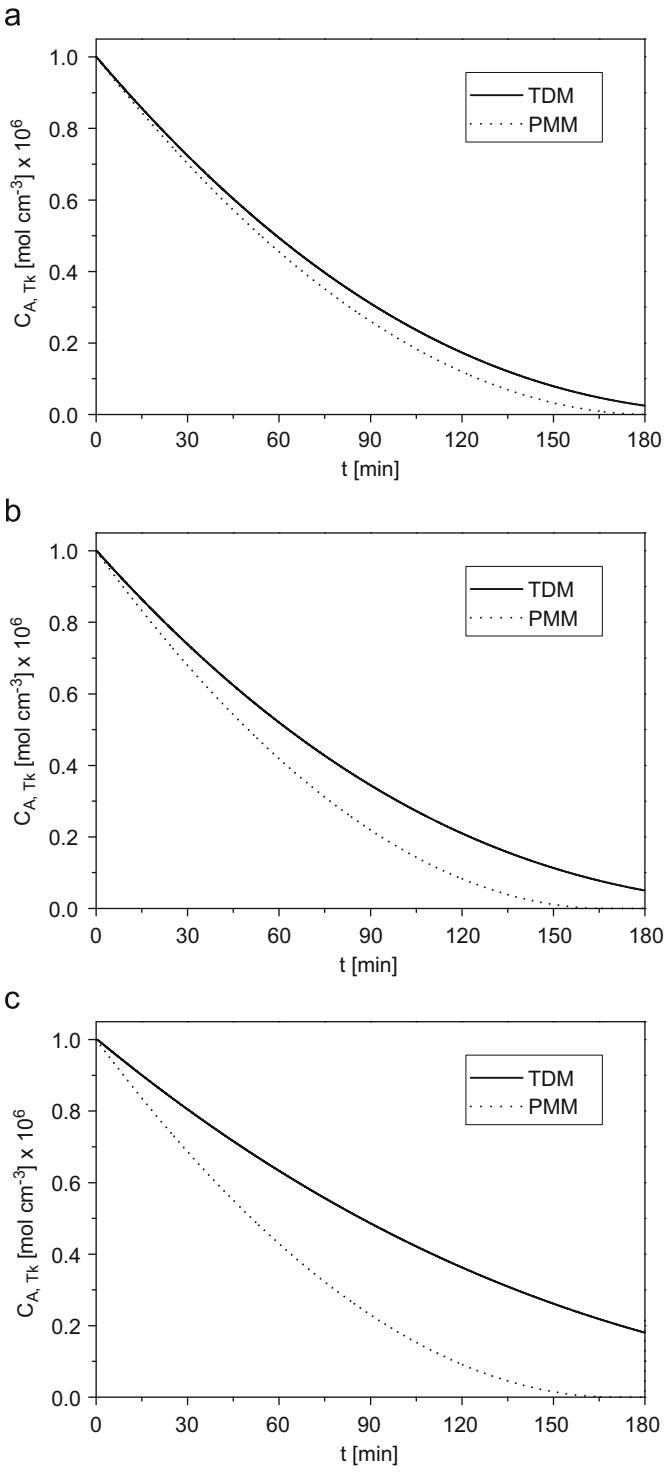

Fig. 10. Tank DCA concentration evolution. Comparison between the TDM and PMM models. $C_A^0=1\times10^{-6}$ mol cm^{-3}; Irradiation level: 100%; $Q=13\,cm^3\,s^{-1}$; $C_{mc}=3.0\times10^{-3}\,g\,cm^{-3}$. (a) $H_R=0.5$ cm.; $V_R=60\,cm^3$. (b) $H_R=1$ cm; $V_R=120\,cm^3$. (c) $H_R=2$ cm; $V_R=240\,cm^3$.

unavoidable or even imposed by the reacting system), (2) high irradiance rates (that can be safely controlled almost always) and low flow rates (that can also be corrected at the expense of a decrease in conversion obtained in the photoreactor). These results are particularly useful for designing laboratory reactors experiments aimed at obtaining intrinsic kinetic parameters.

Nomenclature

A	area (cm^2)
a_V	solid–liquid interfacial area per unit reactor volume ($cm^2\,cm^{-3}$)
a_{V_p}	solid–liquid interfacial area per unit particle volume ($cm^2\,cm^{-3}$)
C_A	molar concentration of component A ($mol\,cm^{-3}$)
C_{mc}	mass concentration of catalyst ($g\,cm^{-3}$)
$\mathcal{D}_{A,mix}$	pseudo-binary diffusion coefficient ($cm^2\,s^{-1}$)
e^a	local volumetric rate of photon absorption ($Einstein\,s^{-1}\,cm^{-3}$)
e_S^a	local superficial rate of photon absorption ($Einstein\,s^{-1}\,cm^{-2}$)
f	spectral emission energy distribution of the lamp (dimensionless)
g	parameter in the phase function for scattering (dimensionless)
H	reactor depth (cm)
I	specific radiation intensity ($Einstein\,s^{-1}\,cm^{-2}\,sr^{-1}$)
L	length (cm)
p	phase function (dimensionless)
q	radiative flux ($Einstein\,s^{-1}\,cm^{-2}$)
Q	volumetric flow rate ($cm^3\,s^{-1}$)
r	radial coordinate (cm)
R	radius (cm)
R_{het}	heterogeneous reaction rate ($mol\,s^{-1}\,cm^{-2}$)
R_{V_p}	reaction rate per unit particle volume ($mol\,s^{-1}\,cm^{-3}$)
Re	Reynolds number (dimensionless)
s	spatial coordinate along a given direction of radiation propagation (cm)
S_g	specific catalyst surface area ($cm^2\,g^{-1}$)
t	time (s)
T	transmittance (dimensionless)
v	velocity ($cm\,s^{-1}$)
V	volume (cm^3)
W	width (cm)
y	cartesian coordinate (cm)
z	cartesian coordinate (cm)

Greek Letters

α_1	kinetic parameter [$cm\,s^{-1}$]
α_2	kinetic parameter ($mol\,s\,Einstein^{-1}\,cm^{-1}$)
β	volumetric extinction coefficient (cm^{-1})
ε	porosity (dimensionless)
η	effectiveness factor (dimensionless)
κ	volumetric absorption coefficient (cm^{-1})
λ	wavelength (nm)
μ	$\cos\theta$ (dimensionless)
μ_0	cosine of the angle between an incoming and a scattered ray (dimensionless)
θ	spherical coordinate (rad)
ρ	density ($g\,cm^{-3}$)
σ	volumetric scattering coefficient (cm^{-1})
ω	σ/β=albedo (dimensionless)
Ω	solid angle (sr)
$\underline{\Omega}$	unit vector in the direction of radiation propagation (dimensionless)

Subscripts

0	global
A	dichloroacetic acid (DCA)
att	attenuation
c	catalyst
diff	diffusion
ex	exit condition
het	heterogeneous
HG	Henyey and Greenstein
in	inlet condition
max	maximum value
P	particle or agglomerate
R	reactor
S	solid or superficial variable
T	total
tk	tank
W	wall of the reactor
z	relative to z-axis
λ	wavelength
$\underline{\Omega}$	direction of radiation propagation

Superscripts

*	specific properties
0	initial value; also surface at $y=0$
H_R	surface at $y=H_R$

Special symbols

$\langle\,\rangle$	average value over a defined space

Acknowledgements

Thanks are given to Universidad Nacional del Litoral, CONICET and Agencia Nacional de Promoción Científica y Tecnológica for financial help. M.M. Ballari acknowledges CONICET for the awarded doctoral fellowship. In addition, the authors wish to express their thanks to Dr. R.J. Brandi, Eng. G. Rintoul, Mr. R. Saavedra, and Mr. A. Negro for their collaboration. The technical assistance of Eng. Claudia Romani is also recognized.

References

Ahmed, S., Ollis, D., 1984. Solar photoassisted catalytic decomposition of the chlorinated hydrocarbons trichloroethylene and trichloromethane. Solar Energy 32 (5), 597–601.

Alfano, O.M., Cabrera, M.I., Cassano, A.E., 1994. Modeling of light scattering in photochemical reactors. Chemical Engineering Science 49, 5327–5346.

Bahnemann, D., 1999. Photocatalytic detoxifications of polluted waters. In: The Handbook of Environmental Chemistry. Vol. 2, Part L: Environmental Photochemistry. Springer-Verlag, Berlin.

Ballari, M.M., Brandi, R.J., Alfano, O.M., Cassano, A.E., 2008a. Mass transfer limitations in photocatalytic reactors employing titanium dioxide suspensions: I. Concentration profiles in the bulk. Chemical Engineering Journal 136, 50–65.

Ballari, M.M., Brandi, R.J., Alfano, O.M., Cassano, A.E., 2008b. Mass transfer limitations in photocatalytic reactors employing titanium dioxide suspensions: II. External and internal particle constrains for the reaction. Chemical Engineering Journal 136, 242–255.

Ballari, M.M., Alfano, O.M., Cassano, A.E., 2009. Photocatalytic degradation of dichloroacetic acid. A kinetic study with a mechanistically based reaction model. Industrial and Engineering Chemistry Research 48 (4), 1847–1858.

Bangun, J., Adesina, A.A., 1998. The photodegradation kinetics of aqueous sodium oxalate solution using TiO_2 catalyst. Applied Catalysis A: General 175, 221–235.

Bideau, M., Claudel, B., Faure, L., Kazouan, H., 1994. Diffusional limitations in liquid phase photocatalysis. Progress in Reaction Kinetics 19, 195–209.

Brandi, R.J., Citroni, M.A., Alfano, O.M., Cassano, A.E., 2003. Absolute quantum yields in photocatalytic slurry reactors. Chemical Engineering Science 58, 979–985.

Cabrera, M.I., Alfano, O.M., Cassano, A.E., 1996. Absorption and scattering coefficients of titanium dioxide particulate suspensions in water. The Journal of Physical Chemistry 100, 20043–20050.

Camera-Roda, G., Santarelli, F., 2007. Optimization of the thickness of a photocatalytic film on the basis of the effectiveness factor. Catalysis Today 129, 161–168.

Cassano, A.E., Martín, C.A., Brandi, R.J., Alfano, O.M., 1995. Photoreactor analysis and design: fundamentals and applications. Industrial and Engineering Chemistry Research 34, 2155–2201.

Chen, D., Ray, A.K., 1999. Photocatalytic kinetics of phenol and its derivatives over UV irradiated TiO_2. Applied Catalysis B: Environmental 23, 143–157.

Chen, D., Li, F., Ray, A.K., 2000. Effect of mass transfer and catalyst layer thickness on photocatalytic reaction. AIChE Journal 46 (5), 1034–1045.

Chen, D., Li, F., Ray, A.K., 2001. External and internal mass transfer effect on photocatalytic degradation. Catalysis Today 66, 475–485.

Chen, J., Ollis, D.F., Rulkens, W.H., Bruning, H., 1999. Photocatalyzed oxidation of alcohols and organochlorides in the presence of native TiO_2 and metallized TiO_2 suspensions. Part (II): photocatalytic mechanisms. Water Research 33, 669–676.

Choi, H., Antoniou, M.G., Pelaez, M., De La Cruz, A.A., Shoemaker, J.A., Dionysiou, D.D., 2007. Mesoporous nitrogen-doped TiO_2 for the photocatalytic destruction of the cyanobacterial toxin microcystin-LR under visible light irradiation. Environmental Science and Technology 41, 7530–7535.

De Lasa, H., Serrano, B., Salaices, M., 2005. Photocatalytic Reaction Engineering. Springer Science, New York.

Dijkstra, M.F.J., Michorius, A., Panneman, H.J., Beenackers, A.A.C.M., 1999. Development of a continuous photocatalytic reactor; slurry versus immobilized. Conference Proceedings, Hungarian Journal of Industrial Chemistry 1, 15–17.

Dijkstra, M.F.J., Buwalda, H., de Jong, A.W.F., Michorius, A., Winkelman, J.G.M., Beenackers, A.A.C.M., 2001a. Experimental comparison of three reactor designs for photocatalytic water purification. Chemical Engineering Science 56, 547–555.

Dijkstra, M.F.J., Michorius, A., Buwalda, H., Panneman, H.J., Winkelman, J.G.M., Beenackers, A.A.C.M., 2001b. Comparison of the efficiency of immobilized and suspended systems in photocatalytic degradation. Catalysis Today 66, 487–494.

Dijkstra, M.F.J., Panneman, H.J., Winkelman, J.G.M., Kelly, J.J., Beenackers, A.A.C.M., 2002. Modeling the photocatalytic degradation of formic acid in a reactor with immobilized catalyst. Chemical Engineering Science 57, 4895–4907.

Dijkstra, M.F.J., Koerts, E.C.B., Beenackers, A.A.C.M., Wesselingh, L.A., 2003. Performance of immobilized photocatalytic reactors in continuous mode. AIChE Journal 49 (3), 734–744.

Dionysiou, D.D., Suidan, M.T., Baudin, I., Laîné, J.M., 2002. Oxidation of organic contaminants in a rotating disk photocatalytic reactor: reaction kinetic in the liquid phase and the role of mass transfer based on the dimensionless Damköhler number. Applied Catalysis B: Environmental 38, 1–16.

Duderstadt, J., Martin, W., 1979. Transport Theory. Wiley, New York.

Edwards, M.E., Villa, C.M., Hill, C.G., Chapman, T.W., 1996. Effectiveness factor for photocatalytic reactions occurring in planar membranes. Industrial and Engineering Chemistry Research 35, 712–720.

Fabiyi, M.E., Skelton, R.L., 1999. The application of oscillatory flow mixing to photocatalytic wet oxidation. Journal of Photochemistry and Photobiology A: Chemistry 129, 17–24.

Goetz, V., Cambon, J.P., Sacco, D., Plantard, G., 2009. Modeling aqueous heterogeneous photocatalytic degradation of organic pollutants with immobilized TiO_2. Chemical Engineering and Processing 48, 532–537.

Gonçalves, M.S.T., Oliveira-Campos, A.M.F., Pinto, E.M.M.S., Plasência, P.M.S., Queiroz, M.J.R.P., 1999. Photochemical treatment of solutions of Azo Dyes containing TiO_2. Chemosphere 39 (5), 781–786.

Hoffmann, M.R., Martin, S.T., Choi, W., Bahnemann, D.W., 1995. Environmental applications of semiconductor photocatalysis. Chemical Review 95, 69–96.

Ilisz, I., László, Z., Dombi, A., 1999. Investigation of the photodecomposition of phenol in near-UV-irradiated aqueous TiO_2 suspensions. I: Effect of charge-trapping species on the degradation kinetics. Applied Catalysis A: General 180, 25–33.

Li Puma, G., Yue, P.L., 1999. Enhanced photocatalysis in a pilot laminar falling film slurry reactor. Industrial and Engineering Chemistry Research 38, 3246–3254.

Malato, S., Blanco, J., Vidal, A., Alarcón, D., Maldonado, M.I., Cáceres, J., Gernjak, W., 2003. Applied studies in solar photocatalytic detoxification: an overview. Solar Energy 75 (4), 329–336.

Martin, C.A., Camera-Roda, G., Santarelli, F., 1999. Effective design of photocatalytic reactors: influence of radiative transfer on their performance. Catalysis Today 48, 307–313.

Matthews, R.W., 1986. Photo-oxidation of organic material in aqueous suspensions of titanium dioxide. Water Research 20 (5), 569–578.

Matthews, R.W., 1991. Environment: photochemical and photocatalytic processes. Degradation of organic compounds. In: Pelizzetti, E., Schiavello, M. (Eds.), Photochemical Conversion and Storage of Solar Energy. Kluwer Academic Publishers, Netherlands, pp. 427–449.

Mehrotra, K., Yablonsky, G.S., Ray, A.K., 2003. Kinetic studies of photocatalytic degradation in a TiO_2 slurry system: distinguishing working regimes and determining rate dependences. Industrial and Engineering Chemistry Research 42, 2273–2281.

Murov, S., Carmichal, I., Hayon, E., 1993. Handbook of Photochemistry, 2nd ed Marcel Dekker, New York.

Ollis, D.F., Pellizzetti, E., 1991. Destruction of water contaminants. Environmental Science and Technology 25 (9), 1523–1529.

Özisik, M.N., 1973. Radiative Transfer and Interactions with Conduction and Convection. Wiley, New York.

Peralta Muniz Moreira, R.F., Sauer, T.P., Casaril, L., Humeres, E., 2005. Mass transfer and photocatalytic degradation of leather dye using TiO_2/UV. Journal of Applied Electrochemistry 35, 821–829.

Preis, S., Krichevskaya, M., Kharchenko, A., 1997. Photocatalytic oxidation of aromatic aminocompounds in aqueous solutions and groundwater from abandoned military bases. Water Science and Technology 35 (4), 265–272.

Ray, A.K., Beenackers, A.A.C.M., 1997. Novel swirl flow reactor for kinetic studies of semiconductor photocatalysis. AIChE Journal 43 (10), 2571–2578.

Reid, R.C., Prausnitz, J.M., Poling, B.E., 1987. The Properties of Gases and Liquid, 4th ed Mc Graw-Hill Book Company, New York.

Sagawe, G., Satuf, M.L., Brandi, R.J., Muschner, J., Federer, C., Alfano, O.M., Bahnemann, D., Cassano, A.E., 2010. Analysis of photocatalytic reactors employing the photonic efficiency and the removal efficiency parameters: degradation of radiation absorbing and nonabsorbing pollutants, Industrial and Engineering Chemistry Research, in press, doi:10.1021/ie901753k.

Salinaro, A., Serpone, N., 1999. Terminology, relative photonic efficiencies and quantum yields in heterogeneous photocatalysis. Part II: experimental determination of quantum yields. Pure and Applied Chemistry 71 (2), 303–320.

Satuf, M.L., Brandi, R.J., Cassano, A.E., Alfano, O.M., 2005. Experimental method to evaluate the optical properties of aqueous titanium dioxide suspensions. Industrial and Engineering Chemistry Research 44, 6643–6649.

Satuf, M.L., Brandi, R.J., Cassano, A.E., Alfano, O.M., 2007. Quantum efficiencies of 4-chlorophenol photocatalytic degradation and mineralization in a well-mixed slurry reactor. Industrial and Engineering Chemistry Research 46, 43–51.

Sclafani, A., Brucato, A., Rizzuti, L., 1993. Mass transfer limitation in a packed bed photoreactor used for phenol removal. In: Ollis, D.F., Al-Ekabi, H. (Eds.), Photocatalytic Purification and Treatment of Water and Air. Elsevier, Amsterdam, pp. 533–545.

Serpone, N., 1997. Relative photonic efficiencies and quantum yields in heterogeneous photocatalysis. Journal of Photochemistry and Photobiology A: Chemistry 104, 1–12.

Siegel, R., Howell, J.R., 2002. Thermal Radiation Heat Transfer, 4th ed Hemisphere Publishing Corp., Bristol.

Stafford, U., Gray, K., Kamat, P.V., 1997. Photocatalytic degradation of 4-chlorophenol: the effects of varying TiO_2 concentration and light wavelength. Journal of Catalysis 167, 25–35.

Subramanian, V., Kamat, P.V., Wolf, E.E., 2003. Mass transfer and kinetic studies during the photocatalytic degradation of an azo dye on optically transparent electrode thin film. Industrial and Engineering Chemistry Research 42, 2131–2138.

Turchi, C.S., Ollis, D.F., 1988. Photocatalytic reactor design: an example of mass transfer limitations with an immobilized catalyst. Journal of Physical Chemistry 92, 6852–6853.

Turchi, C.S., Ollis, D.F., 1989. Mixed reactant photocatalysis: intermediates and mutual rate inhibition. Journal of Catalysis 119, 483–496.

Van de Hulst, H.C., 1980. Multiple Light Scattering. Academic Press, New York.

Wei, T.Y., Wan, C.C., 1991. Heterogeneous photocatalytic oxidation of phenol with titanium dioxide powders. Industrial and Engineering Chemistry Research 30, 1293–1300.

Zalazar, C.S., Labas, M.D., Martín, C.A., Brandi, R.J., Alfano, O.M., Cassano, A.E., 2005. The extended use of actinometry in the interpretation of photochemical reaction engineering data. Chemical Engineering Journal 109, 67–81.

Zhou, S., Ray, A.K., 2003. Kinetic studies for photocatalytic degradation of eosin b on a thin film of titanium dioxide. Industrial and Engineering Chemistry Research 42, 6620–6633.